Annals of Botany **101**: 187–195, 2008
doi:10.1093/aob/mcm283, available online at www.aob.oxfordjournals.org

OXFORD JOURNALS
OXFORD UNIVERSITY PRESS

TECHNICAL ARTICLE

Nanoparticles as Smart Treatment-delivery Systems in Plants: Assessment of Different Techniques of Microscopy for their Visualization in Plant Tissues

P. GONZÁLEZ-MELENDI[1,†,‡], R. FERNÁNDEZ-PACHECO[2,†], M. J. CORONADO[1], E. CORREDOR[1], P. S. TESTILLANO[1], M. C. RISUEÑO[1], C. MARQUINA[1], M. R. IBARRA[2,3], D. RUBIALES[4] and A. PÉREZ-DE-LUQUE[4,*]

[1]*Centro de Investigaciones Biológicas, CSIC, Ramiro de Maeztu 9, E-28040 Madrid, Spain,* [2]*Instituto de Nanociencia de Aragón, Universidad de Zaragoza, Edificio Interfacultativo II, Pedro Cerbuna 12, 50009-Zaragoza, Spain,* [3]*Instituto de Ciencia de Materiales de Aragón-Departamento de Física de la Materia Condensada, CSIC-Unversidad de Zaragoza, Pedro Cerbuna 12, 50009-Zaragoza, Spain and* [4]*CSIC, Instituto de Agricultura Sostenible, Alameda del Obispo s/n, Apdo. 4084, E-14080 Córdoba, Spain*

Received: 31 July 2007 Returned for revision: 3 September 2007 Accepted: 20 September 2007 Published electronically: 12 November 2007

• *Background and Aims* The great potential of using nanodevices as delivery systems to specific targets in living organisms was first explored for medical uses. In plants, the same principles can be applied for a broad range of uses, in particular to tackle infections. Nanoparticles tagged to agrochemicals or other substances could reduce the damage to other plant tissues and the amount of chemicals released into the environment. To explore the benefits of applying nanotechnology to agriculture, the first stage is to work out the correct penetration and transport of the nanoparticles into plants. This research is aimed (*a*) to put forward a number of tools for the detection and analysis of core-shell magnetic nanoparticles introduced into plants and (*b*) to assess the use of such magnetic nanoparticles for their concentration in selected plant tissues by magnetic field gradients.
• *Methods Cucurbita pepo* plants were cultivated *in vitro* and treated with carbon-coated Fe nanoparticles. Different microscopy techniques were used for the detection and analysis of these magnetic nanoparticles, ranging from conventional light microscopy to confocal and electron microscopy.
• *Key Results* Penetration and translocation of magnetic nanoparticles in whole living plants and into plant cells were determined. The magnetic character allowed nanoparticles to be positioned in the desired plant tissue by applying a magnetic field gradient there; also the graphitic shell made good visualization possible using different microscopy techniques.
• *Conclusions* The results open a wide range of possibilities for using magnetic nanoparticles in general plant research and agronomy. The nanoparticles can be charged with different substances, introduced within the plants and, if necessary, concentrated into localized areas by using magnets. Also simple or more complex microscopical techniques can be used in localization studies.

Key words: Nanotechnology, nanoparticles, drug delivery, smart delivery systems, microscopy techniques.

INTRODUCTION

The emergence of nanotechnology and the development of new nanodevices and nanomaterials (Scott and Chen, 2003; Joseph and Morrison, 2006) open up potential novel applications in agriculture and biotechnology.

Nanoparticles are materials that are small enough to fall within the nanometric range, with at least one of their dimensions being less than a few hundred nanometres. This reduction in size brings about significant changes in their physical properties with respect to those observed in bulk materials. Most of these changes are related to the appearance of quantum effects as the size decreases, and are the origin of phenomena such as the superparamagnetism, Coulomb blockade, surface plasmon resonance, etc. The increase in the surface area to volume ratio is also a consequence of the reduction in size. It leads to the appearance of surface effects related to the high number of surface atoms, as well as to a high specific area, which are important from the practical point of view. A wide variety of materials can be used to make such nanoparticles, such as metal oxide ceramics and silicates, magnetic materials, lyposomes, dendrimers, emulsions, etc. (for a review, see Holister *et al.*, 2003). There are a large variety of methods that can be used to in the production of nanoparticles, making use of techniques from both physics and chemistry. Among the first ones, arc-discharge, high-energy ball milling, laser pyrolysis and laser ablation are the most commonly used. Electrochemical and chemical vapour deposition, sonochemistry and different wet chemistry routes (e.g. sol-gel, co-precipitation, inverse micelles, etc.) are also widely employed.

A very interesting application of nanoparticles in the scope of life sciences is their use as 'smart' delivery systems. They were already postulated in 1906 by the Nobel Prize winner P. Ehrlich as 'magic bullets' (see

* For correspondence. E-mail bb2pelua@uco.es
† Both authors contributed equally to this work.
‡ Present address: Centro de Biotecnología y Genómica de Plantas, Universidad Politécnica de Madrid, E.T.S. Ingenieros Agrónomos, Ciudad Universitaria s/n, 28040-Madrid, Spain.

Himmelweit, 1960), and are usually nanoparticles loaded with a drug or therapeutic agent. In addition, some specific property and/or external modification of these nanoparticles allows their accumulation and/or guidance into specific areas within a living organism in which the chemical charge will be unloaded, and avoids the immunogenic response that would clear these nanoparticles from circulation. Presently, these smart delivery systems are being widely investigated for cancer treatments (Kukowska-Latallo *et al.*, 2005). Their ability to target specifically the desired tumour tissue avoids the undesired side-effects of the treatment and reduces the concentration of drug required, leading to a more efficient drug administration.

The first systems selected for preliminary assays were carbon-coated magnetic nanoparticles (De Teresa *et al.*, 2005; Fernández-Pacheco *et al.*, 2005). Nanoparticles are currently being widely investigated for targeted delivery of drugs in cancer treatments (Alexiou *et al.*, 2000, 2005). The magnetic core allows allocation of the nanoparticles to the place of interest (affected tissues) using small magnets. Also, carbon encapsulation provides biocompatibility and a large adsorption surface. Thus, different types of molecules can be adsorbed onto the carbon layers (De Teresa *et al.*, 2005; Fernández-Pacheco *et al.*, 2005). It is also possible to functionalize and/or conjugate particle coatings with different biomolecules (chemicals, enzymes, etc.), a fact that is of great interest for their use as smart delivery systems.

There is a huge scope for applying nanoparticles and nanocapsules to plants for agricultural use (Liu *et al.*, 2001*a–c*; Pavel *et al.*, 1999; Cotae and Creanga, 2005; Pavel and Creanga, 2005; Joseph and Morrison, 2006). Gene transfer by bombardment of DNA-absorbed gold particles has been successfully used to generate transgenic plants in a species-independent manner (Christou *et al.*, 1988). Recently, Torney *et al.* (2007) reported the efficient delivery of DNA and chemicals through silica nanoparticles internalized in plant cells, without the requirement of specialized equipment. To achieve this efficiently, a study on the ways penetration and transport work inside the whole plant, tissues and cells is needed. The goal of this research is the development and application of microscopy tools and techniques at different levels of resolution, which are easily available in most research institutes, to visualize and track the transport and deposition of nanoparticles inside the plants, and also to check the possibility of concentrating magnetic nanoparticles into localized areas of the plants using small magnets. This preliminary study of the application of carbon-coated magnetic nanoparticles in whole living plants is reported here for the first time.

MATERIALS AND METHODS

Plant material and growth conditions

Pumpkin (*Cucurbita pepo*) plants were selected for preliminary experiments due to the large size of their vessels, which would facilitate the transport of nanoparticles through the vascular system. Plants were grown using a polyethylene bag system previously described (Pérez-de-Luque *et al.*, 2006) (Fig. 1A). A strip (11 × 28 cm) of glass-fibre paper (Whatmann GF/A) was inserted in a polyethylene bag (25 × 35 cm). Pumpkin seeds were germinated in Petri dishes on moistened filter paper. Pumpkin seedlings (15-d old) with a radicle length of about 4–5 cm were transferred to the bag, placing them on the upper side of the system. Twenty millilitres of Hoagland nutrient solution (Hoagland and Arnon, 1950) was added to each bag, and refilled later when necessary. The bags were suspended vertically in boxes and the plants were grown in a controlled environment chamber with a day/night temperature of 20 ± 0·5 °C, a 14-h photoperiod and irradiance of 200 μmol m^{-2} s^{-1}.

Synthesis of nanoparticles

Carbon-coated iron nanoparticles were produced following the discharge arc method (De Teresa *et al.*, 2005; Fernández-Pacheco *et al.*, 2005) based on that previously designed by Krätschmer-Huffman *et al.* (1990). The Krätschmer-Huffman method uses a cylindrical chamber, in which there are two graphite electrodes: a stationary anode containing 10-μm-diameter starting iron powders, and a moveable graphite cathode. An arc is produced between the graphite electrodes in an atmosphere of helium. The graphite electrode is sublimed and builds up a powder deposit (soot) on the inner surface of the chamber. In this material, carbon nanostructures, amorphous carbon and iron and iron oxides nanoparticles encapsulated in graphitic layers were found, together with a small amount of non-coated or partially coated metallic particles. These particles (which are not biocompatible) were eliminated by chemical etching, washing the soot with 3 M HCl at 80 °C. This procedure favours the formation of carboxylic groups on the graphitic shell, which, due to their hydrophobic nature, will contribute to the stability of the final particle suspension. In order to eliminate the amorphous carbon and therefore increase the concentration of magnetic nanoparticles, a magnetic purification of the powder is carried out. For this purpose, stable suspensions of the particles are prepared in a surfactant solution: 2·5 g of SDS in 500 mL of distilled water. A field gradient produced by a 3KOe permanent magnet was used for magnetic separation of this suspension.

Application of nanoparticles

Nanoparticles were suspended in gelafundine, a commercial succinated gel, and the solution was kept in water in an ultrasonic bath for several minutes. This solution was selected as a preliminary approach because it is used in animal experiments (Fernández-Pacheco *et al.*, 2007). A biocompatible magnetic fluid was obtained in this way, which was used to inoculate the plants. The method selected, which favours the penetration of nanoparticles into the plants, involved injecting the bioferrofluid inside the internal hollow of the leaf petiole (Fig. 1B). In this way, the bioferrofluid penetrates into the plant and is translocated to other areas through the vascular tissues. Small magnets were placed on the petiole of the leaf opposite to the injection point and on some of the roots (Fig. 1A, B).

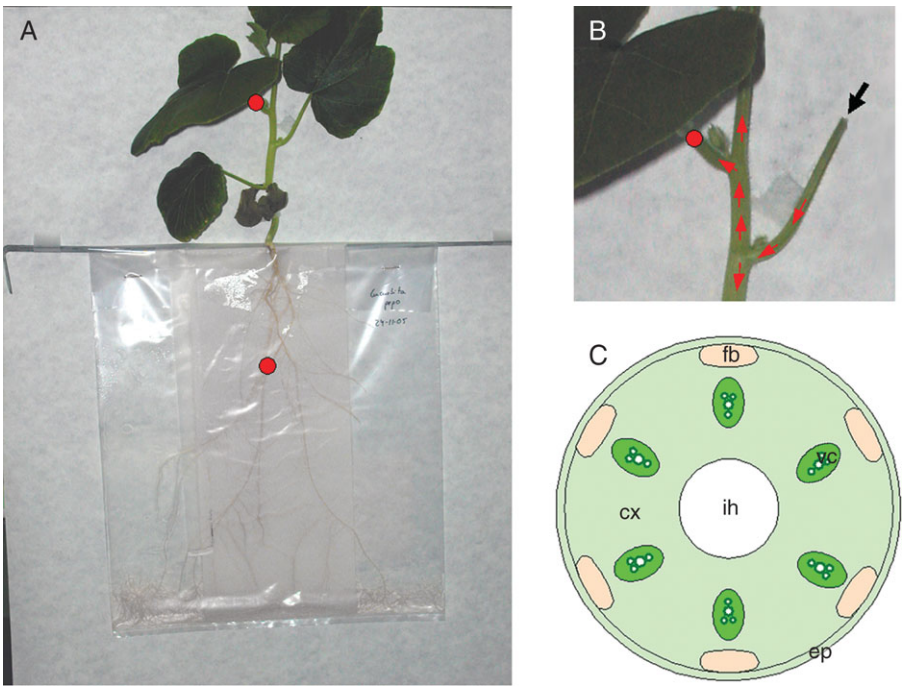

FIG. 1. (A) Pumpkin plant growing in the polyethylene bag system. Red circles indicate where magnets were placed. (B) Detail showing the point of application of the bioferrofluid (black arrow) and further expected movement of nanoparticles through the vascular system (red arrows). (C) Schematic representation of a transverse section of the pumpkin stem. ep, Epidermis; cx, cortex; fb, fibres; vc, xylem vessels; ih, internal hollow.

Collection and processing of samples for microscopy analysis

Stem and petiole samples at the application point of the nanoparticles were collected 24, 48 and 72 h after application of the bioferrofluid. Roots and petiole samples were also collected before, after and at the point of the magnet localization. The samples were fixed in Karnovsky solution (4 % formaldehyde + 5 % glutaraldehyde, in 0·025 M cacodilate buffer, pH 6·9) for 4 h at room temperature and then were kept in buffer at 4 °C. The samples were treated in one of three ways: (1) cut by hand and observed using light microscopy; (2) cut with a vibratome and observed under a confocal laser scanning microscope; or (3) embedded either in paraffin or Epon resin, then sectioned with a microtome or ultramicrotome and observed on a light or electron microscope.

For paraffin embedding, the samples were dehydrated in an ethanol series (50, 80, 95, 100, 100 %; 12 h each) and transferred to an embedding solvent (xylene; Panreac Quimica S.A., Montcada i Reixac, Spain) through a xylene–ethanol series (30, 50, 80, 100, 100 %; 12 h each) and finally saturated with paraffin (Paraplast Xtra; Sigma, St Louis, MO, USA). Sections (7 μm thick) were cut with a rotary microtome (Nahita 534; Auxilab S.A., Beriain, Spain) and attached to adhesive-treated microscope slides (polylysine slides; Menzel GmbH & Co KG, Braunschweig, Germany).

For the confocal laser scanning microscope, 40-μm sections were cut under water in a vibratome (vibratome series 1000; Intracel, Royston, Herts, UK), collected and mounted on slides with a mixture of PBS : glycerol (1:1).

For resin embedding and further light and electron microscopy analysis, approx. 1-mm-thick, hand-cut cross-sections were dehydrated through an ethanol series (30, 50, 70 and 100 %) and were then treated with propylene oxide and infiltrated with Epon resin (Serva, Heidelberg, Germany) according to the manufacturer's directions. Polymerization in capsules was performed overnight at 60 °C. Semi-thin sections (1–2 μm) and ultra-thin sections (70–90 nm) were cut from the blocks and observed under light and electron microscopes, respectively.

Microscopy analysis methods

Hand-cut sections were observed directly on a light microscope (Leica DM-LB, magnification × 100–400; Leica Microsystems Wetzlar GmbH, Wetzlar, Germany) and photographed using a digital camera (Nikon DXM1200F; Nikon Europe B.V., Badhoevedorp, The Netherlands).

Paraffin sections (7 μm) were attached to adhesive-treated microscope slides (polylysine slides; Menzel GmbH & Co KG). After removal of paraffin with xylene (20 min twice) and rehydration with an ethanol–water series (100, 100, 95, 70, 50, 30, 0 %; 20 min each), the sections were dried on a hot plate at 45 °C for 1 h, mounted with DePeX (BDH) and observed under phase contrast and epifluorescence at 450–490 nm (blue-violet) excitation wavelength on the microscope referred to above.

Stacks of confocal optical sections from vibratome sections were collected using a Leica TCS-SP2-AOBS-UV spectral confocal laser scanning microscope (Leica

Microsystems Wetzlar GmbH). The presence of nanoparticles was detected either by differential interference contrast or reflection. For the latter, the specimens were excited with the Ar laser line of 488 nm and the reflected signal was collected in the range 485–500 nm.

For correlative microscopy, 1- to 2-μm sections were cut from the polymerized blocks, observed on a light photomicroscope (Leitz, Germany) under phase contrast, bright field and dark field, and photographed using an Olympus DC10 digital camera. Small trapezoid areas containing plant tissues with nanoparticles, as identified on the sections observed on the light microscope, were trimmed down on the surface of the blocks using a Piramitome device (LKB). From these trapezoid areas, 100-nm sections were cut on an ultramicrotome (Reichert, Germany) and collected on 200-mesh nickel grids. The sections on the grids were stained with a solution of 5 % uranyl acetate in water for 30 min, washed in water, dried and observed on a transmission electron microscope (Jeol 1010). Micrographs were taken with a Megaview digital camera (Gatan). The size of the particles detected on the electron microscope was determined on a representative number of images. The diameter of 890 particles was measured, grouped in consecutive intervals spanning 10 nm and the relative frequencies were represented in a histogram.

RESULTS

Different imaging methods, at the resolutions of light and electron microscopy, have been tested to detect the presence of nanoparticles inside plant tissues. Basically, two approaches have been followed: (1) observation of thick sections of tissues under either fluorescence or confocal microscopy; and (2) examination of thin and ultra-thin sections from resin-embedded specimens on conventional light and transmission electron microscopes. These cover a wide range of detection techniques using non-sophisticated equipment of increasing availability in most research institutes.

A schematic representation of the transverse section of the pumpkin stem is presented in Fig. 1C, with the distribution of tissues as a guide to the location of the spatial position of the regions shown in Figs 2–4.

Concentration of bioferrofluid by application of a magnetic field gradient

The first question to assess was whether the nanoparticles would penetrate into the living plant and travel through the vascular system to the places where the magnets were located. Figure 2 shows how the bioferrofluid penetrated at the application point (Fig. 2A) and was later located in other parts of the plant, including the roots (Fig. 2B, D and E). The magnets concentrated the bioferrofluid in the vascular tissues adjacent to their location in both petiole (Fig. 2B) and roots (Fig. 2E). The intense dark coloration corresponding to the accumulation of bioferrofluid was not detected in vascular areas opposite to the magnet placement of the same sections (Fig. 2C) or in samples located after the magnet placement (Fig. 2F).

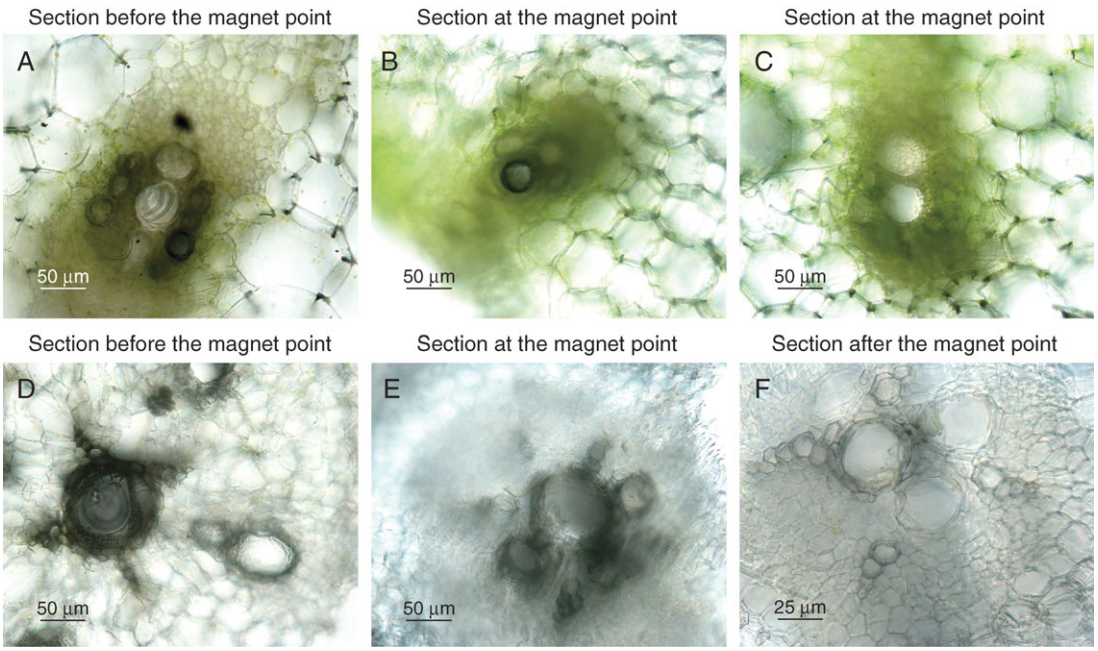

FIG. 2. Hand-cut sections of petioles (A–C) and roots (D–F) of pumpkin plants treated with bioferrofluid. (A) Detail of vascular tissues at the application point. Dark coloration indicates accumulation of bioferrofluid. (B) Detail of vascular tissues adjacent to a magnet. Bioferrofluid is concentrated in xylem vessels. (C) Detail of vascular tissues opposite a magnet placement. No bioferrofluid accumulation is observed. (D) Detail of root vascular tissue preceding magnet localization. Bioferrofluid appears distributed through the xylem vessels as a dark staining. (E) As (D) but at the point of the magnet placement. Again strong presence of bioferrofluid is observed. (F) As (D) but after the point of the magnet placement. No bioferrofluid is observed, indicating its flux was mainly stopped at the magnet placement.

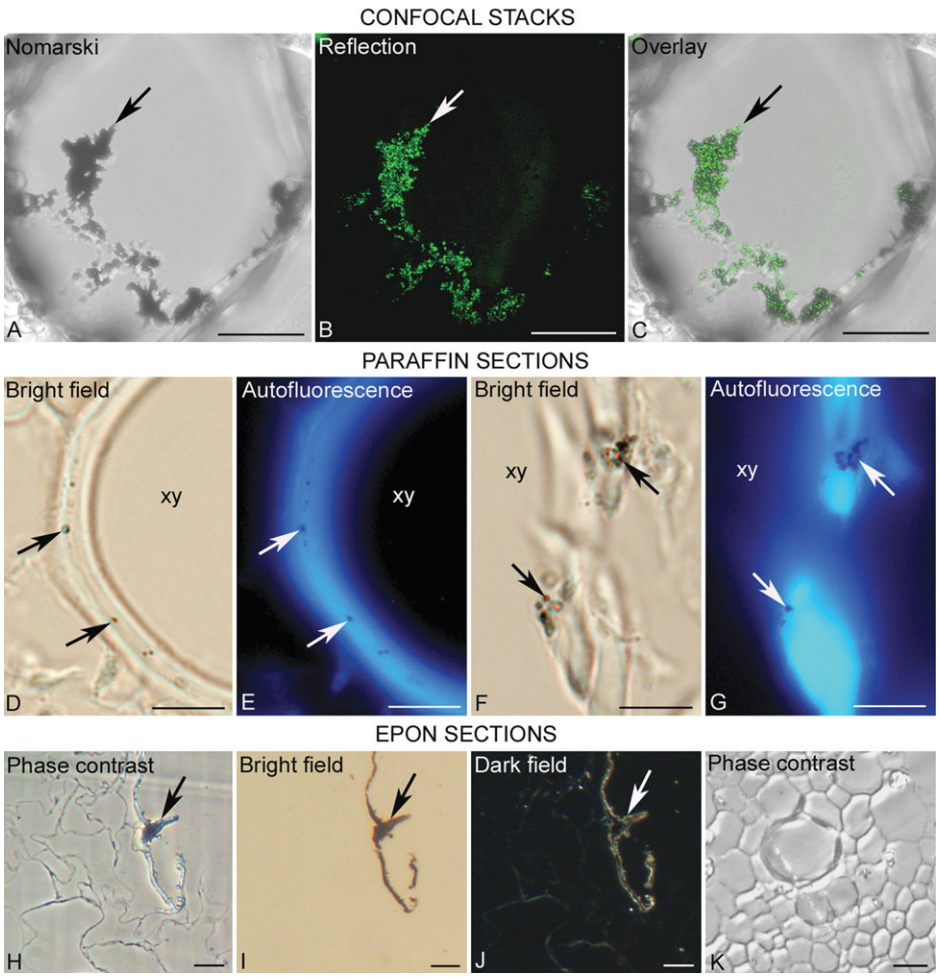

FIG. 3. Techniques for the detection of nanoparticles injected into plants at the resolution of the light microscope. (A–C) Projection of 3-D confocal stacks from a cell of the stem, after 72 h at the position of the magnet. Aggregates of nanoparticles (arrow) are detected by Nomarski (A) and reflection (B) techniques. The overlay between (A) and (B) is shown in (C) with an almost complete colocalization. (D–G) Detection of nanoparticles on 7-μm sections of paraffin-embedded plant tissues. The particles, identified as dark dots under bright field (arrows in D and F) correspond to non-fluorescent areas (arrows in E and G) within the autofluorescent cell wall of xylem cells (xy) under an epi-fluorescence microscope. (H–K) Detection of nanoparticles on 1- to 2-μm sections from specimens embedded in Epon resin, after 24 h at the site of injection. The nanoparticles can be observed on a light photomicroscope as a punctuate pattern of dark or refringent areas (arrows) under phase contrast (H), bright field (I) and dark field (J). (K) shows a portion of the stem with a xylem vessel from a control plant without any signal, under phase contrast. Scale bar = 10 μm.

Imaging of nanoparticles on the confocal and fluorescence microscopes

Although the nanoparticles used in this study have a diameter size within the nanometre range, thus below the resolution limit of the light microscope, aggregates of different sizes were formed in the solution where the particles were suspended, even after sonication. These aggregates of nanoparticles in the solution, before application into the plants, were visualized by the differential interference contrast or Nomarski technique and were also revealed when the samples were excited with an Ar laser and the reflected signal collected in a narrow range of the spectrum that includes the excitation wave length on 3-D confocal stacks (data not shown). The same methods were applied to locate the presence of nanoparticles in the plant tissues. Figure 3A–C shows nanoparticles inside a cell of the cortex next to the internal hollow of the petiole just before the position of the magnet, 72 h after the injection, as detected by the Nomarski (Fig. 3A) and reflection (Fig. 3B) techniques on the confocal microscope. Figure 3C shows the overlay of Fig. 3A and B. Solutions without nanoparticles and untreated plant controls did not provide any signal (data not shown).

Figure 3D–G show the presence of nanoparticles associated with the cell wall of the xylem vessel cells, naturally autofluorescent due to their major component, lignin. The nanoparticles identified under bright field (arrows in Fig. 3D, F) can be seen as non-autofluorescent dots in the cell wall (arrows in Fig. 3E, G).

Imaging of nanoparticles on correlative light and electron microscopy analysis

Some specimens were embedded in a resin for correlative light and electron microscopy studies. The first level of

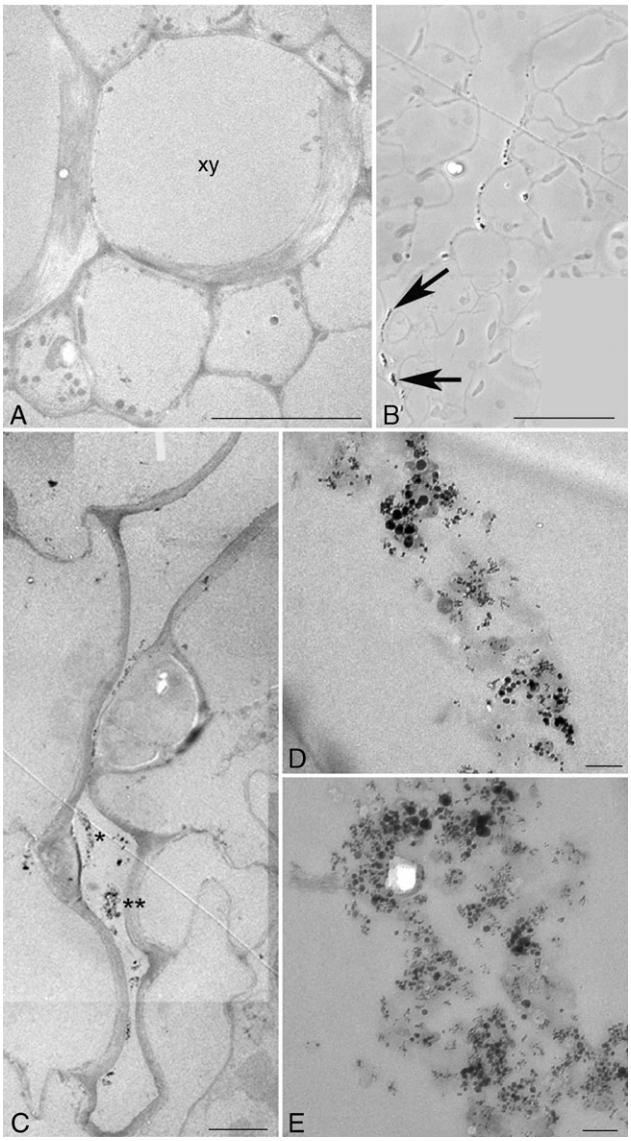

FIG. 4. Transmission electron microscopy. (A) A similar area of the cortex to the one shown in Fig. 3K, with a section of a xylem cell (xy). No particles are detected. (B–E) Nanoparticles detected on correlated light and electron microscopy imaging of the same specimen after 24 h at the injection site. (B) The nanoparticles (arrows) are seen as beads on a string along the cells on the outer side of the cell wall at a groove of the epidermis by phase contrast on a light microscope. (C) The same area as in (B) imaged on the transmission electron microscope where electron-dense areas can be seen (asterisks): (D, E) higher magnification of the areas marked in (C) with one and two asterisks, respectively, in which aggregates of nanoparticles of different sizes can clearly been recognized in the extracellular area. Scale bars: A = 10 μm; B = 50 μm; C = 5 μm; D, E = 0·1 μm.

analysis was the observation of 1- to 2-μm sections on the light microscope to search for the presence of nanoparticles. Under phase contrast, an opaque signal was observed inside some cells and attached to the outer side of the cell wall of the cells surrounding the internal hollow of the petiole (arrow in Fig. 3H) after 24 h at the injection site. Under bright field, the structural details of the cells on unstained sections was lost but the same pattern as that detected in Fig. 3H was clearly observed (arrow in Fig. 3I) and under dark field, as refringent areas, as well (arrow in Fig. 3J). On sections from untreated control plants, that pattern was not observed either under phase contrast (Fig. 3K), bright field or dark field (data not shown).

The same regions observed on the light microscope were analysed under the electron microscope as described in Materials and methods. Since the nanoparticles have a core of iron, these would be expected to be directly seen at the resolution of the electron microscope. No particles were detected on control sections (Fig. 4A). At the injection site, 24 h after the treatment, aggregates of dense material were detected in a groove of the epidermis and in the extracellular space in between cells of the epidermal layer, on a light microscope under phase contrast (Fig. 4B) and bright and dark fields (data not shown). A correlative analysis on the electron microscope unambiguously revealed numerous nanoparticles close together (Fig. 4C); these would correspond to the aggregates observed on the light microscope. A high magnification of the asterisk-marked regions in Fig. 4C shows that individual round-shaped nanoparticles can be clearly resolved (Fig. 4D, E). To give contrast in the ultra-thin sections for electron microscopy, uranyl acetate only was used, thus avoiding counterstaining with lead citrate, which eventually could form small precipitates of a similar size to that of the nanoparticles.

The diameter of the nanoparticles detected on the electron microscope was measured. The data were grouped in consecutive intervals spanning 10 nm and the relative frequencies were represented in a histogram (Fig. 5). The distribution of sizes corresponded to sections of the nanoparticles at different levels with maximum values at 50 nm. However, these nanoparticles in solution have been characterized with a diameter ranging from 5 to 200 nm (Fernández-Pacheco *et al.*, 2005).

DISCUSSION

In this work, different processing approaches were used with the aim of providing a range of technical alternatives

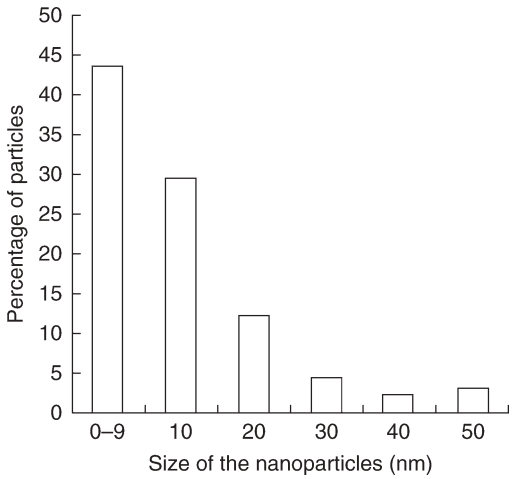

FIG. 5. Size distribution of nanoparticles found in the cells and the extracellular space after injection.

that different laboratories can adapt to their equipment. All of the alternatives hereby presented have been proven valid for the observation of nanoparticles in plant tissues and cells. Aggregation of metal particles, with a diameter size within the micrometer range, in the culture medium and internalization into human osteoblasts have been reported by Vallés *et al.* (2007) by reflection on a confocal microscope. In the present study, the Nomarski and reflection techniques on the confocal microscope have proved to be sufficiently sensitive to detect the aggregates formed by nanoparticles, thus providing a reliable methodological approach for their visualization. Since reflection requires the collection of the emitted signal in a very narrow range of the spectrum including the excitation wavelength, this technology is restricted to state-of-the art spectral confocal microscopes, which permit control over where the signal is collected. These microscopes have been on the market for over 5 years and their availability in most research institutes is increasing. Non-spectral confocals would provide images overlapping reflection and (auto)fluorescence. Then, the use of these microscopes for nanoparticle detection would only be suitable in those specimens with a low autofluorescence signal. The aggregates formed by the nanoparticles were also observed within 3-D stacks spanning cortex cells. Thus, the confocal analysis demonstrates the internalization of nanoparticles inside plant tissues. Whether or not the aggregates of nanoparticles are formed in the cytoplasm, presumably by converging carriers of smaller groups of particles which have not been taken up, is still unknown. It cannot be ruled out that some particles are washed out during the manipulation of the specimens (chopping off the plant material, fixing, washing and further processing). Then, those particles identified in the present work must reflect strong interactions and/or retention in the plant tissues.

Autofluorescence, either natural or induced by glutaraldehyde fixation, can be used to infer the presence of nanoparticles as dark areas embedded within a fluorescent background. This approach had been successfully applied to detect the internalization of micrometric metal particles and aggregates into human macrophages (Vallés *et al.*, 2006) and osteoblasts (Vallés *et al.*, 2007). However, most plant cells are highly vacuolated with reduced dense cytoplasmic areas, thus making the identification of deposits of nanoparticles, apart from specific structures and cell types not always evident. Only some particles associated with the cell wall of xylem vessels, which are highly autofluorescent due to their major component – lignin – were observed.

Different resins can be used to embed fixed specimens depending on their final use and the resolution level of the observations. Paraffin embedding is commonly used for light microscopy analysis. Epoxi and acrylic resins, such as Epon, LRWhite or Lowicryl permit the correlation between light and electron microscopy observations, but usually require protocols that last up to 1 week (González-Melendi *et al.*, 2005). In this work, a correlative approach was followed by observing semi-thin and ultrathin sections on the light and electron microscopes, respectively, collected from the same blocks of specimens embedded in Epon resin. Dark and refringent small signals were seen on the light microscope, which were further identified as iron-core nanoparticles on the electron microscope.

As far as is known, to date there has not been any report about penetration and transport of nanoparticles inside whole plants. The most recent paper dealing with this topic appeared recently in *Nature Nanotechnology* (Torney *et al.*, 2007), but the work was limited to isolated plant cells and intact leaves. Here, it has been shown how magnetic nanoparticles can penetrate into the plant and the bioferrofluid travels through the vascular system to other parts of the plant, and how this bioferrofluid can be concentrated in the desired areas by using magnets. Since no particles with a diameter size bigger than 50 nm have been detected inside plant tissues, a size-based selection mechanism seems to be operating, probably involving cell walls and waxes acting as a barrier. More studies are underway to unveil the penetration mechanisms of the nanoparticles inside the plant and plant cells, and their transportation and movement to and through the vascular system.

Many things must be addressed prior to utilization of nanoparticles in agriculture. First, those concerning the plant physiology and growth in mid- and long-term, i.e. do the nanoparticles significantly affect the plant and are they phytotoxic? Damage in the plants used during the present experiments was not observed. Furthermore, some of the treated plants were transplanted in pots and grown until maturity like normal plants. It is possible that nanoparticles produce some local damage in cells, as has been reported for *in vitro* treatments (Pavel *et al.*, 1999; Cotae and Creanga, 2005; Pavel and Creanga, 2005), but it does not mean that the whole plant would be affected. However, phytotoxicity of more intense treatments should not be discarded, and specific assays must be done in this way. Secondly, the effect of nanoparticles entering the food chain must be considered and studied. There are recent reports about cytotoxicity of nanoparticles developed for biomedical applications (Brunner *et al.*, 2006; Panessa-Warren *et al.*, 2006), but no studies about their effect after entering the digestive system are available nor are there any considering whole organisms.

With respect to the use of magnetic nanoparticles in a large-scale situation, it is impractical to place magnets in annual extensive crops (e.g. cereals). But it would be possible for specific treatments in fruit trees (e.g. olive trees) or high-input crops under greenhouse conditions. However, the main advantage of using magnetic nanoparticles is in laboratory and research applications because they allow a very precise localization of the particles to unload their charge, which is of great interest in the study of local treatments in whole living plants. Nevertheless, nanoparticles lacking magnetic properties could be used in large-scale situations with extensive crops, designed with other systems which allow their accumulation and/or guidance into specific areas. In that case, field applications could be done through the leaves and/or root system.

In conclusion, bioferrofluids can be introduced into whole living plants, can travel using the vascular system and can be concentrated in specific areas by application

of magnetic gradients. In this work, a number of microscopy tools to identify the tissue and subcellular location of nanoparticles in plants is also described. These cover a range of reliable methodological approaches based on fluorescence, confocal, light and electron microscopy which can be selected by the research teams to achieve their scientific goals within their technical availabilities and skills. In summary, nanoparticles can be visualized by reflection on a confocal microscope; inferred as dark areas in an autofluorescent background (either natural or induced), although with some limitations depending on the cell types and as a dense signal on the light microscope, further identified as clusters of nanoparticles on the electron microscope, due to their iron core. The preliminary results of the present work showed the presence of nanoparticles both in the extracellular space and within some cells. Further work is needed to evaluate how the nanoparticles penetrate and are transported within the plants, and the mechanism(s) of intracellular internalization to explore the potential of nanoparticles as smart treatment-delivery systems in plants.

ACKNOWLEDGEMENTS

A. Pérez de Luque acknowledges a post-doctoral contract at the IAS-CSIC funded by the programme 'Ramón y Cajal' of the Spanish Ministry of Education and Science. M. J. Coronado is funded by the programme 'Juan de la Cierva' of the Spanish Ministry of Education and Science. P. González-Melendi is funded by the programme 'Ramón y Cajal' of the Spanish Ministry of Education and Science. We thank Alicia Rodríguez Huete for helping in the preparation of the specimens for electron microscopy and María Teresa Seisdedos and Silvia Hernández from the service of the confocal microscopy of the CIB. This research was supported by the project NanoAgro-200540F0041 funded by CSIC (Proyectos Intramurales de Frontera) and by the project NAN2004-09270-C03-03 funded by the Spanish Strategic Action on Nanoscience and Nanotechnology of the Spanish Ministry of Education and Science.

LITERATURE CITED

Alexiou C, Wolfgang A, Klein RJ, Parak FG, Hulin P, Bergemann C, *et al*. 2000. Locoregional cancer treatment with magnetic drug targeting. *Cancer Research* **60**: 6641–6648.

Alexiou C, Jurgons R, Schmid R, Hilpert A, Bergemann C, Parak F, *et al*. 2005. *In vitro* and *in vivo* investigation of targeted chemotherapy with magnetic nanoparticles. *Journal of Magnetism and Magnetic Materials* **293**: 389–393.

Brunner TJ, Wick P, Manser P, Spohn P, Grass RN, Limbach LK, *et al*. 2006. *In vitro* cytotoxicity of oxide nanoparticles: comparison of asbestos, silica, and the effect of particle solubility. *Environmental Science and Technology* **40**: 4374–4381.

Christou P, McCabe DE, Swain WF. 1988. Stable transformation of soybean callus by DNA-coated gold particles. *Plant Physiology* **87**: 671–674.

Cotae V, Creanga I. 2005. LHC II system sensitivity to magnetic fluids. *Journal of Magnetism and Magnetic Materials* **289**: 459–62.

De Teresa JM, Marquina C, Serrate D, Fernández-Pacheco R, Morellon L, Algarabel PA, *et al*. 2005. From magnetoelectronic to biomedical applications based on the nanoscale properties of advanced magnetic materials. *International Journal of Nanotechnology* **2**: 3–22.

Fernández-Pacheco R, Ibarra MR, Valdivia JG, Marquina C Serrate D, Romero MS, *et al*. 2005. Carbon coated nanoparticles for local drug delivery using magnetic implants. In: Laudon M, Romanowicz B, eds. *Technical Proceedings of the 2005 NSTI Nanotechnology Conference and Trade Show*, Vol. 1. Anaheim, CA: Nano Science and Technology Institute, 144–147.

Fernández-Pacheco R, Marquina C, Valdivia JG, Gutiérrez M, Romero MS, Cornudella R, *et al*. 2007. Magnetic nanoparticles for local drug delivery using magnetic implants. *Journal of Magnetism and Magnetic Materials* **311**: 318–322.

González-Melendi P, Ramírez C, Kumlehn J, Testillano PS, Risueño MC. 2005. 3D confocal and electron microscopy imaging define the dynamics and mechanisms of diploidisation at early stages of barley microspore-derived embryogenesis. *Planta* **222**: 47–57.

Himmelweit F. (ed). 1960. *The collected papers of Paul Ehrlich*, Vol. 3. London: Pergamon Press.

Hoagland DR, Arnon DI. 1950. *The water-culture method for growing plants without soil*. California Agricultural Experiment Station Circular No. 347.

Holister P, Weener JW, Román Vas C, Harper T. 2003. Nanoparticles. *Technology White Papers* **3**: 1–11. Available online at http://images.iop.org/dl/nano/wp/nanoparticles_WP.pdf

Johnson J, Kent T, Koda J, Peterson C, Rudge S, Tapolsky G. 2002. The MTC technology: a platform technology for the site-specific delivery of pharmaceutical agents. *European Cells & Materials Journal* **3**: 12–15.

Joseph T, Morrison M. 2006. *Nanotechnology in agriculture and food*. www.nanoforum.org

Kratschmer W, Lamb LD, Fostiropoulos K, Huffman DR. 1990. Solid C_{60} a new form of carbon. *Nature* **347**: 354–358.

Kukowska-Latallo JF, Candido KA, Cao Z, Nigavekar SS, Majoros IJ, Thomas TP, Balogh LP, Khan MK, Baker JR Jr. 2005. Nanoparticle targeting of anticancer drug improves therapeutic response in animal model of human epithelial cancer. *Cancer Research* **65**: 5317–5324.

Linke KH, Joel DM, Kroschel J. 2001. Observations of the underground development: polybag system. In: Kroschel J, ed. *A technical manual for parasitic weed research and extension*. Dordrecht: Kluwer Academic Publishers, 56–58.

Liu Y, Laks P, Heiden P. 2002*a*. Controlled release of biocides in solid wood. I. Efficacy against brown rot wood decay fungus (*Gloeophyllum trabeum*). *Journal of Applied Polymer Science* **86**: 596–607.

Liu Y, Laks P, Heiden P. 2002*b*. Controlled release of biocides in solid wood. II. Efficacy against *Trametes versicolor* and *Gloeophyllum trabeum* wood decay fungi. *Journal of Applied Polymer Science* **86**: 608–614.

Liu Y, Laks P, Heiden P. 2002*c*. Controlled release of biocides in solid wood. III. Preparation and characterization of surfactant-free nanoparticles. *Journal of Applied Polymer Science* **86**: 615–621.

Panessa-Warren BJ, Warren JB, Wong SS, Misewich JA. 2006. Biological cellular response to carbon nanoparticle toxicity. *Journal of Physics: Condensed Matter* **18**: 2185–2201.

Pavel A, Creanga DE. 2005. Chromosomal aberrations in plants under magnetic fluid influence. *Journal of Magnetism and Magnetic Materials* **289**: 469–472.

Pavel A, Trifan M, Bara II, Creanga DE, Cotae C. 1999. Accumulation dynamics and some cytogenetical tests at *Chelidonium majus* and *Papaver somniferum* callus under the magnetic liquid effect. *Journal of Magnetism and Magnetic Materials* **201**: 443–445.

Pérez-de-Luque A, Lozano MD, Cubero JI, González-Melendi P, Risueño MC, Rubiales D. 2006. Mucilage production during the incompatible interaction between *Orobanche crenata* and *Vicia sativa*. *Journal of Experimental Botany* **57**: 931–942.

Scott N, Chen H. 2003. *Nanoscale science and engineering for agriculture and food systems*. Washington, DC: Cooperative State Research, Education and Extension Service, United States Department of Agriculture.

Torney F, Trewyn BG, Lin V S-Y, Wang K. 2007. Mesoporous silica nanoparticles deliver DNA and chemicals into plants. *Nature Nanotechnology* **2**: 295–300.

Vallés G, González-Melendi P, González-Carrasco JL, Saldaña L, Sánchez-Sabaté E, Munuera L, *et al*. 2006. Differential inflammatory macrophage response to rutile and titanium particles. *Biomaterials* **27**: 5199–5211.

Vallés G, González-Melendi P, Saldaña L, Rodríguez M, Munuera L, Vilaboa N. 2007. Rutile and titanium particles differentially affect the production of osteoblastic local factors. *Journal of Biomedical Materials Research Part A*. DOI: 10·1002/jbm.a.31363. Available online at http://www3.interscience.wiley.com/cgi-bin/abstract/114286309/ABSTRACT